Mechanics & Industry **19**, 306 (2018)

https://doi.org/10.1051/meca/2018026

Mechanics & Industry

Available online at:
www.mechanics-industry.org

Regular Article

Mesh stiffness modeling considering actual tooth profile geometry for a spur gear pair

Yong Yang[1], Jiaxu Wang[1,2], Qinghua Zhou[1,*], Yanyan Huang[1], Jinxuan Zhu[1], and Wanyou Yang[1]

[1] School of Aeronautics and Astronautics, Sichuan University, Chengdu 610065, PR China
[2] State Key Laboratory of Mechanical Transmissions, Chongqing University, Chongqing 400044, PR China

Received: 15 June 2017 / Accepted: 3 May 2018

Abstract. Some tooth profile geometric features, such as root fillet area, flank modification and wear are of nonnegligible importance for gear mesh stiffness. However, due to complexity of analytical description, their influence on mesh stiffness was always ignored by existing research works. The present work derives analytical formulations for time-varying gear mesh stiffness by using parametric equations of flank profile. Tooth geometry formulas based upon a rack-type tool are derived following Litvin's vector approach. The root fillet area and tooth profile deviations can therefore be fully considered for spur gear tooth stiffness evaluation. The influence of gear fillet determined by tip fillet radius of the rack-type tool is quantified parametrically. The proposed model is validated to be effective by comparing with a finite element model. Further, the model is applied to investigate the stiffness variations produced by tooth addendum modification, tooth profile nonuniform wear and modification.

Keywords: Mesh stiffness / root fillet curve / tooth profile modification / addendum modification / nonuniform wear

1 Introduction

Health monitoring and fault diagnosis of a gear transmission system are always conducted based on its dynamic characteristics, wherein vibration is widely recognized as the most important one. Elastic deformation on engaged teeth, determined by the coupled effect between the distributed load on contacting teeth and gear mesh stiffness, is one of the main reasons leading to vibration in a gear transmission system [1]. However, when applying a constant load, the load distribution between two contacting tooth pairs is directly related to mesh stiffness. Furthermore, the variations of teeth number in contact and mesh position during meshing result in a changing gear mesh stiffness, inducing extra complexity on mesh stiffness calculation. Therefore, accurate and effective calculation of meshing stiffness is of great importance to gear dynamics [2–4].

In ISO standard 6336-2 [5] and AGMA standard 2001-D04 [6], Navier's equation was applied for cylindrical gear bending calculation based upon assuming the load is uniformly distributed along the line of contact. It is known that the load distribution is usually different at each contact point and it depends on the meshing stiffness. In order to obtain better evaluation of gear mesh stiffness and load sharing, both finite element method (FEM) and analytical method have been adopted. Numerous works have been published [7–11] by taking the benefit of the FEM. Lin et al. [10] developed a three-dimensional (3D) FEM to derive mesh stiffness and tooth load distribution under both static and dynamic loading during meshing process. Ma et al. [11] established a finite element model for a spur gear pair in meshing. Time-varying mesh stiffness (TVMS) under different crack depths was then obtained based on the proposed model. The FEM has been proved to be able to obtain pretty accurate evaluation of gear mesh stiffness. However, related operation utilizing the FEM is time-consuming and difficult to model [12,13].

On the other hand, analytical methods provide simple and effective ways to calculate tooth stiffness, which were adopted by many researchers. Pedrero et al. [14] proposed a non-uniform load distribution model along the line of contact for involute external gears by employing the minimum elastic potential energy criterion. Chaari, Fakhfakh and Haddar [13] derived an analytical formulation for mesh stiffness of spur gears based upon the widely used Weber equation. However, their research did not provide detailed method on specific tooth profile geometry modeling. Fernandez et al. [15] used an analytical approach, combined with the FEM, to formulate the deformation at each contact point on the gear tooth.

* e-mail: qh.zhou@foxmail.com

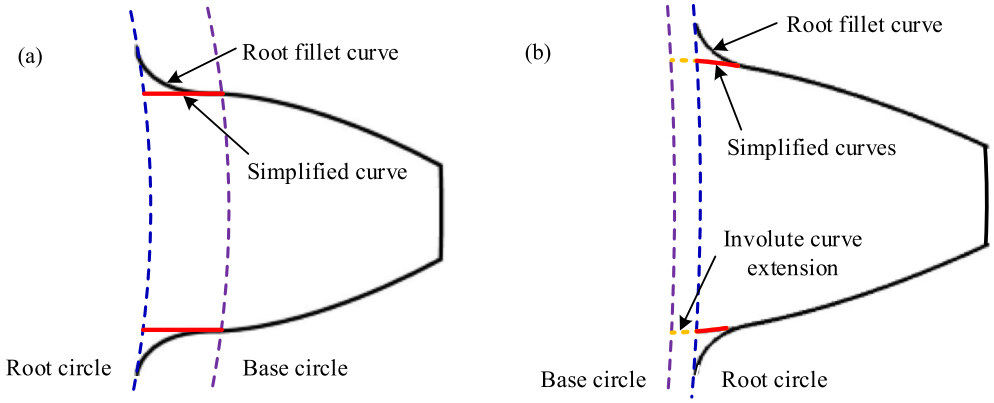

Fig. 1. Tooth modeling: (a) root circle is smaller than base circle (R-B tooth), (b) root circle is bigger than base circle (B-R tooth).

The meshing stiffness can therefore be obtained accordingly. Ma et al. [16] studied the influence of torque variation on the mesh stiffness by using a newly proposed analytical method and FEM. Yang and Lin [17] introduced a potential energy method to compute the stiffness for mating gear teeth by considering bending, axial compressive and Hertzian contact stiffnesses. Further, Tian et al. [18] thought that the shear stiffness should also be considered to enhance the method proposed by Yang and Lin [17]. The improved potential energy method was then utilized by Saxena et al. [19] to investigate the influence of time-varying friction coefficient on the total effective mesh stiffness for spur gear pairs, by Liang et al. [12] to evaluate the mesh stiffness of a planetary gear set. In most of existing related studies, the gear body was treated as rigid; very few research works have modeled the gear as elastic body to investigate the influence of gear-body deformation on mesh stiffness. Sainsot and Velex [20] assumed that stress variations at dedendum circle were linear and constant, and then developed an analytical formula for gear body-induced tooth deflection. Nevertheless, the research on actual tooth profile geometry modeling and its effect on gear mesh stiffness is limited. This study focuses on actual tooth profile geometry, i.e., root fillet area, profile modification and wear, and investigation of its effect on the TVMS.

When computing the mesh stiffness of a spur gear pair, the gear tooth was usually modeled as a cantilever beam that starts from the base circle without root fillet curve [4,17,18]. Actually, as shown in Figure 1a and b, the gear tooth starts from the root circle. When the base circle is bigger than root circle (such tooth is defined as "R-B tooth" in the present work), the models in the above work ignored the gear tooth part between the base and root circles. However, when base circle is smaller than root circle (defined as "B-R tooth" instead), the models considered the tooth part of involute curve extension between the two circles. Some other methods [12,21] discussed separately for both the types of gears whose base circles are bigger or smaller than root circle. In the work of Liang et al. [12], a more rigorous cantilever beam model for gear tooth was developed based on the assumption that a gear tooth starts from the root circle. When base circle is smaller or bigger than root circle, they used straight lines, presented by the red lines in Figure 1(a) and (b), respectively, to simplify the root fillet curves. However, the accurate root fillet curves were still not considered. In Ref. [13], the authors thought that the stiffness of a whole tooth from the addendum to dedendum circles can be evaluated by modeling the tooth as a nonuniform cantilever beam with an effective length. But they did not provide the explicit analytical equations of tooth profile. Tooth geometry formulas on the basis of a rack-type tool following Litvin's vector approach [22] were mentioned in Refs. [15,23,24], but the influence of tool tip fillet radius change on meshing stiffness was not discussed. Feng et al. [24] built a uniform wear model to analyze mesh stiffness for gears with tooth wear. But it is known that wear is not as severe at the pitch point as it is on the addendum or dedendum of the tooth. Chen and Shao [25] proposed a method to calculate mesh stiffness of spur gear pairs with tooth profile modification. However, they did not provide the detailed model for mesh stiffness of a single tooth pair with profile deviations.

In this paper, an analytical approach with accurate consideration of tooth root fillet curves and profile deviations is developed to evaluate the gear mesh stiffness. The influence of the tip fillet radius of rack-type tools and addendum modification on gear mesh stiffness is investigated. Some profile deviations, such as tooth profile modification and wear, are further studied for a better understanding of its influence on gear mesh stiffness.

2 Machining tool and its parametric equations

An involute gear tooth profile consists of three parts, i.e., involute profile, root fillet curve and dedendum circle, as shown in Figure 2. A is the intersection point of the dedendum circle and root fillet curve. B is the starting point of the involute profile, as well as the end point of the root fillet. C is the starting point of the contact zone on the tooth flank. D is the tooth end point. Rack cutter or hob is widely used for the generation of spur involute gears in industry. The meshing between a hob and a gear being generated can be considered as a rack-gear meshing. The rotation of the hob is always viewed as the translational movement of the imaginary rack [22]. Figure 3 shows the tooth profile of a

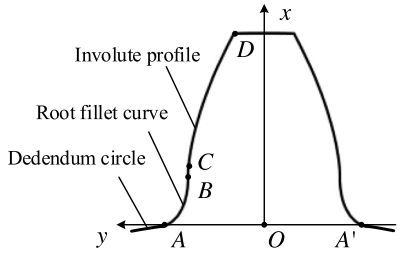

Fig. 2. Tooth profiles of an involute gear.

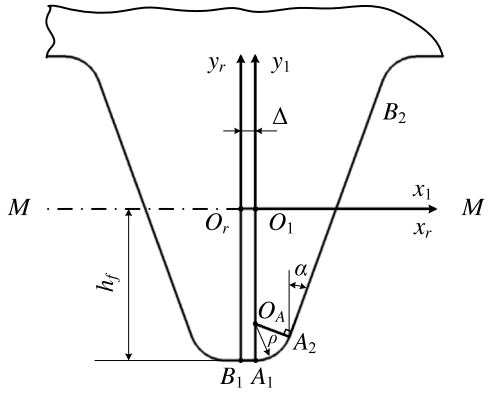

Fig. 3. Tooth shape of a rack-type gear cutter and relative coordinate systems.

rack cutter or the axial section of a hob. Straight line parts A_1B_1 and A_2B_2 on the tool profile generate the dedendum circle and involute profile of the gear tooth, respectively. Part A_1A_2, appeared as an arc with radius ρ and center point O_A, generates the root fillet of the spur gear. ρ not only determines meshing interference and undercut, but also affects the strengths and lives of both the tool and the machined gear.

2.1 Conventional settings of rack-cutter

When a conventional setting of the rack-cutter is employed, the middle-line of a rack-cutter is tangent to the gear pitch circle [26]. In this case, rack-cutter centrode and its middle-line are coincident with each other during the whole cutting process. A two-dimensional (2D) coordinate system $S_r(x_r, y_r)$ is established by setting the centrode as the x_r axis and the symmetrical line of tool tooth as the y_r axis, respectively. Another coordinate system $S_1(x_1, y_1)$ is then introduced with both the two axes parallel to those of coordinate system $S_r(x_r, y_r)$. The center O_A of the arc part A_1A_2 on tool profile locates on the y_1 axis of the latter coordinate, as shown in Figure 3. Some parameters in Figure 3 can be expressed as

$$h_f = (h_a* + c*)m \tag{1}$$

$$\begin{aligned}\Delta &= O_rO_1 \\ &= \pi m/4 - \left[h_f - (1 - \sin\alpha)\rho\right]\tan\alpha - \rho\cos\alpha\end{aligned} \tag{2}$$

where h_f is the dedendum of the machined gear, h_a* and $c*$ denote the addendum and clearance coefficients, respectively, m represents the module; α is the profile angle; Δ is the distance between tool tip fillet arc center and tool symmetric line.

The radius ρ of the arc part on rack-cutter plays a decisive role in the generation of the machined gear root fillet area. The arc A_1A_2 must be tangent to both the straight lines A_2B_2 and A_1B_1. Therefore, the length of A_1B_1 cannot be less than 0. The value of ρ should satisfy the following inequality

$$\rho \le \frac{\cos\alpha}{1 - \sin\alpha}\left(\frac{\pi m}{4} - h_f\tan\alpha\right) \tag{3}$$

To avoid interference between tooth root fillet area and gear tip during meshing, pressure angle of involute profile starting point (point B in Fig. 2) should be less than that of the starting point of the contact zone on tooth profile (point C in Fig. 2). Therefore, the value of ρ should also satisfy

$$\begin{aligned}\rho &\le \frac{1}{1 - \sin\alpha} \\ &\times \left[h_f - \frac{m}{2}\sin\alpha\left(\sqrt{Z_0^2\sin^2\alpha + 4Z_0h_a^* + 4h_a^{*2}} - Z_0\sin\alpha\right)\right]\end{aligned} \tag{4}$$

where Z_0 denotes the number of teeth on the mating gear of the gear being generated.

In order to prevent undercutting, ρ should be greater than the minimum limit [22] expressed as

$$\rho \ge \frac{2h_f - Zm\sin^2\alpha}{2(1 - \sin\alpha)} \tag{5}$$

where Z represents the tooth number of the machined gear. The above contents suggest that the variation range of ρ must greatly shrink in order to satisfy the above three in equations simultaneously.

2.2 Non-conventional settings of rack-cutter

Nonstandard gears are also generated by a standardized tool used for standard gears, but with a modified setting corresponding to the cutting gear [22]. When a modified setting of the rack-cutter is employed, its middle-line M-M moves a distance of $me*$ with respect to the centrode of the rack-cutter. The displacement of the rack-cutter brings a thickness change to gear tooth. The expressions for h_f and Δ become

$$h_f = (h_a^* + c^* - e^*)m \tag{6}$$

$$\begin{aligned}\Delta &= |O_rO_1| \\ &= \pi m/4 - \left[h_f - (1 - \sin\alpha)\rho + e^*m\right]\tan\alpha - \rho\cos\alpha\end{aligned} \tag{7}$$

where $e*$ is the modification coefficient. $e^* > 0$ if the displacement is performed outward from the machined gear center; $e^* < 0$ if the displacement is performed toward the gear center.

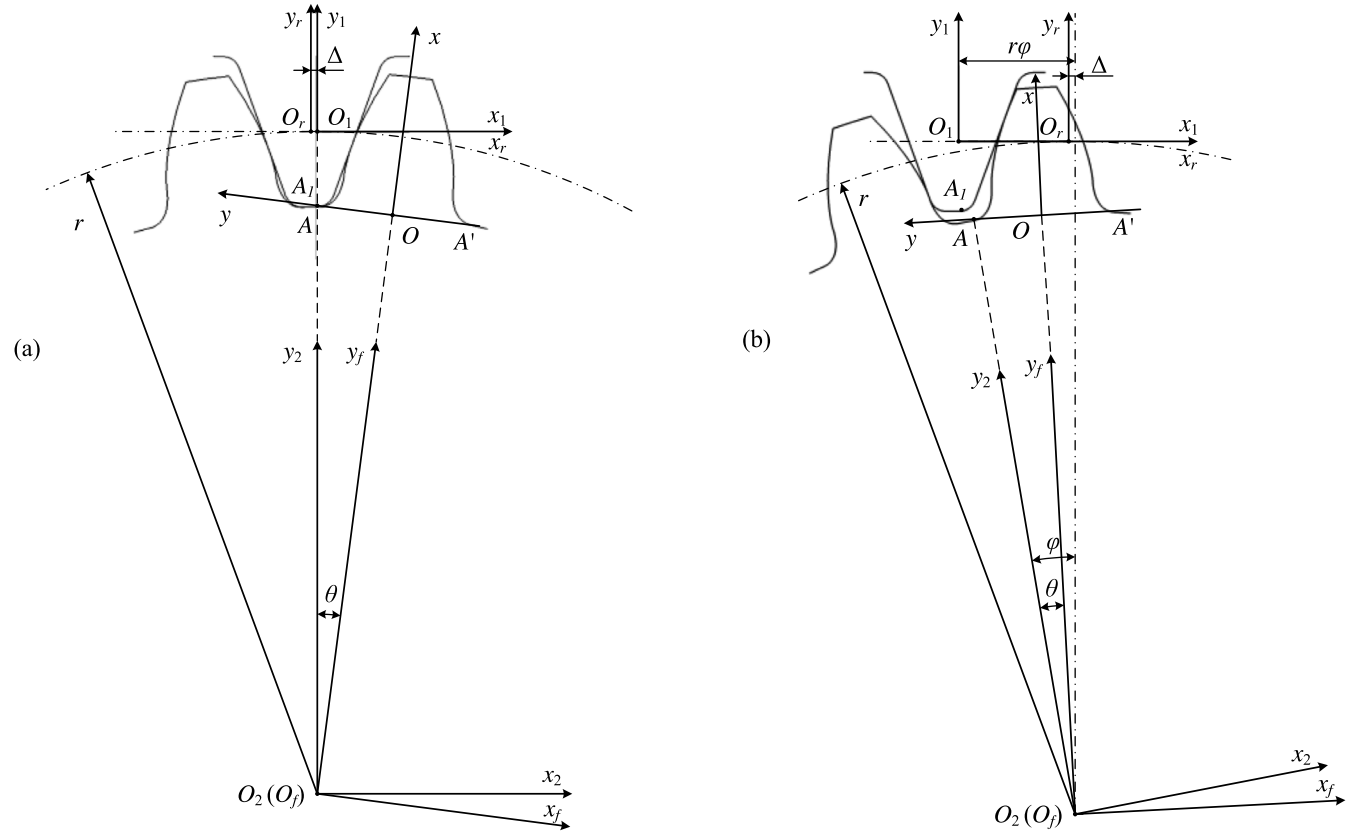

Fig. 4. Derivation of coordinate transformation by rotation: (a) initial position of coordinate systems S_f, S_1, S_2, and S, (b) position of coordinate systems S_f, S_1, S_2, and S when gear rotates φ.

2.3 Equations of a rack-cutter flank profile

In tooth cutting process the rack-cutter reciprocates parallel to the machined gear rotation axis. The gear tooth is shaped into the envelope for the family of rack-cutter shapes which are expressed in coordinate system with rigid connection to the gear being machined [26]. In coordinate system S_1, parametric equations for the arc part A_1A_2 on the rack-cutter are expressed as follows

$$\begin{cases} x_{1r} = u \\ y_{1r} = \rho\sin\alpha - h - \sqrt{\rho^2 - u^2} \end{cases} \quad u \in [0\rho\cos\alpha] \tag{8}$$

The parametric equations for the straight-line portion A_2B_2 of the cutting tool in coordinate system S_1 are given by the following formulas

$$\begin{cases} x_{1l} = u \\ y_{1l} = cot\alpha(u - \rho\cos\alpha) - h \\ u \in [\rho\cos\alpha, (mh_a^* + h)\tan\alpha + \rho\cos\alpha] \end{cases} \tag{9}$$

3 Derivation of gear mesh stiffness considering root fillet area

3.1 Tooth flank profile equations

The schematic for coordinate transformation of gear cutting process is shown in Figure 4. Coordinate system S_1 is rigidly connected to the tool tooth that performs a translational motion with regard to the fixed coordinate system S_r. A detailed description about the two coordinates is demonstrated in Section 2. Coordinate system $S_0(x, y)$ is introduced with setting the symmetrical line of the gear tooth as x axis. The direction of coordinate axis y coincides with $A'A$ (see Fig. 2). $S_2(x_2, y_2)$ and $S_f(x_f, y_f)$ are two coordinate systems rigidly connected to the machined gear with gear center as original point. θ is the angle between coordinate axes y_2 and y_f. The difference is that y_2 and y_f axes are parallel to y_1 and x axes, respectively. The initial position of the coordinate axis y_2 and point A_1 on the rack-cutter coincide with the axis y_1 and point A on the tooth profile, respectively (Fig. 4a). φ is the angle of gear rotation from initial position.

The equations for spur gear tooth profiles involving involute profile and root fillet curve can be derived. The matrices $\mathbf{M}_{21}$, $\mathbf{M}_{f2}$ and $\mathbf{M}_{0f}$ are defined to describe the translations from $S_1(x_1, y_1)$ to $S_2(x_2, y_2)$, $S_2(x_2, y_2)$ to $S_f(x_f, y_f)$ and $S_f(x_2, y_2)$ to $S_0(x, y)$, respectively, which are expressed as follows

$$\mathbf{M}_{21} = \begin{bmatrix} \cos\varphi & \sin\varphi & r(\sin\varphi - \varphi\cos\varphi) \\ -\sin\varphi & \cos\varphi & r(\cos\varphi + \varphi\sin\varphi) \\ 0 & 0 & 1 \end{bmatrix};$$

$$\mathbf{M}_{f2} = \begin{bmatrix} \cos\theta & -\sin\theta & 0 \\ \sin\theta & \cos\theta & 0 \\ 0 & 0 & 1 \end{bmatrix}; \mathbf{M}_{0f} = \begin{bmatrix} 0 & 1 & -L \\ -1 & 0 & 0 \\ 0 & 0 & 1 \end{bmatrix}$$

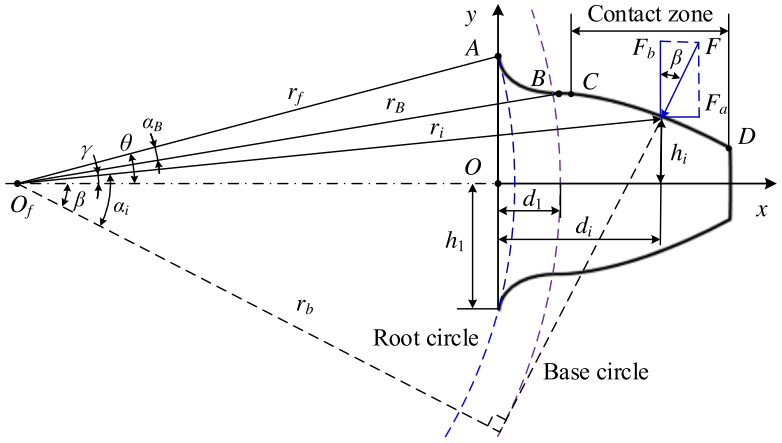

Fig. 5. Beam model of a spur gear tooth.

where

$$\theta = \pi/z - \Delta/r \tag{10}$$

$$L = O_f O = r\cos\theta \tag{11}$$

Accordingly, the transition matrix $\mathbf{M}_{01}$ relating $S_1(x_1, y_1)$ to $S_0(x, y)$ can be obtained

$$\mathbf{M}_{01} = \mathbf{M}_{0f}\mathbf{M}_{f2}\mathbf{M}_{21} \tag{12}$$

The curve equations of gear root fillet, generated by arc part A_1A_2 on the tool profile, can be derived in coordinate system $S_0(x, y)$ through Eqs. (8) and (12).

$$\begin{cases} x_{AB} = (-u + r\varphi)\sin(\varphi - \theta) + (r + \rho\sin\alpha - h \\ \qquad -\sqrt{\rho^2 - u^2})\cos(\varphi - \theta) - L \\ y_{AB} = (-u + r\varphi)\cos(\varphi - \theta) - (r + \rho\sin\alpha - h \\ \qquad -\sqrt{\rho^2 - u^2})\sin(\varphi - \theta) \end{cases} \tag{13}$$

where $\varphi(u) = \frac{(\rho\sin\alpha - h)u}{r\sqrt{\rho^2 - u^2}}$, $u \in [0\ \rho\cos\alpha]$

The involute profile of gear tooth is yielded by part A_1B_1 of the tool profile. According to Eqs. (9) and (12), involute profile equations in coordinate system $S_0(x, y)$ can be expressed by

$$\begin{cases} x_{BD} = (-u + r\varphi)\sin(\varphi - \theta) + [r + cot\alpha(u - \rho\cos\alpha) \\ \qquad -h]\cos(\varphi - \theta) - L \\ y_{BD} = (-u + r\varphi)\cos(\varphi - \theta) - [r + cot\alpha(u - \rho\cos\alpha) \\ \qquad -h]\sin(\varphi - \theta) \end{cases} \tag{14}$$

where $\varphi(u) = [ucsc^2\alpha - (\rho cot\alpha\cos\alpha + h)cot\alpha]/r$, $u \in [\rho\cos\alpha, (mh_a{}^* + h)\tan\alpha + \rho\cos\alpha]$. u can also be expressed as a function of φ

$$u(\varphi) = u = \varphi r\sin^2\alpha + (\rho\cos^2\alpha + h\sin\alpha)\cos\alpha \tag{15}$$

3.2 Equations of tooth profile with deviations

For a gear pair with tooth profile deviations, such as tooth wear and profile modification, its tooth flank equations can be expressed as follows

$$\begin{cases} x'_{BD} = x_{BD} - \Delta h\sin\beta_u \\ y'_{BD} = y_{BD} - \Delta h\cos\beta_u \end{cases} \tag{16}$$

where Δh is the profile normal offset; β_u means the angle between the normal direction of tooth flank and the axis y.

3.3 Potential energy method for gear mesh stiffness

In previous work [8,12,17,18,21], the potential energy method is employed to evaluate the mesh stiffness of fixed-shaft gear pairs with the assumption that the gear system is perfect without friction and transmission error. The same assumptions is also adopted in this paper. The strain energy of a spur tooth, U, can be represented as the sum of bending energy U_b, shear energy U_s, radial compression energy U_a and the Hertzian contact energy U_h, which correspond to bending stiffness k_b, shear stiffness k_s, compression stiffness k_a and Hertzian contact stiffness k_h, respectively. According to elastic mechanics [27], the relations between elastic potential energies and stiffnesses are expressed as

$$U_b = \frac{F^2}{2k_b},\ U_s = \frac{F^2}{2k_s},\ U_a = \frac{F^2}{2k_a},\ U_h = \frac{F^2}{2k_h} \tag{17}$$

where F means the action force at contact point along the action line. As shown in Figure 5, F_a and F_b are two orthogonal components of F.

$$F_a = F\sin\beta,\ F_b = F\cos\beta \tag{18}$$

For an external gear, the gear teeth may be either B-R or R-B teeth. In Refs. [12,21], the two types of teeth were discussed separately. While in this paper, the mesh stiffness of both B-R and R-B teeth can be evaluated by using the same formulas. As shown in Figure 5, r_B denotes the distance from the gear center to the end point B of root fillet curve. Generally, $r_B > r_b$ is satisfied no matter the root circle is smaller or bigger than the base circle. In the following work bending, shear and axial compressive stiffnesses for the two cases will be evaluated by the same formulas, rather than be treated separately as in Ref. [12]. By employing the potential energy method, U_b, U_s and U_a

can be obtained [17,18]

$$U_b = \frac{F^2}{2k_b} = \int_0^{d_i} \frac{[F_b(d_i - x) - F_a h_i]^2}{2EI_x} dx \tag{19}$$

$$U_s = \frac{F^2}{2k_s} = \int_0^{d_i} \frac{1.2{F_b}^2}{2GA_x} dx \tag{20}$$

$$U_a = \frac{F^2}{2k_a} = \int_0^{d_i} \frac{{F_a}^2}{2EA_x} dx \tag{21}$$

where E and G represent elastic and shear moduli, respectively, h_i is the distance from the gear contact point to tooth central line, d_i is the distance between the contact point and the tooth root (the coordinate axis y). A_x and I_x denote respectively the area and the moment of inertia of the cross section at the contact point.

According to the equations of the root fillet and involute curves (i.e., Eqs. (13) and (14)), the above equations can be expressed as follows

$$U_b = \int_0^{\rho\cos\alpha} \frac{[F_b(d_i - x_{AB}(u)) - F_a h_i]^2}{\frac{4}{3}EBy_{AB}^3(u)} \cdot \frac{dx_{AB}(u)}{du} du + \int_{\rho\cos\alpha}^{u(\theta-\gamma)} \frac{[F_b(d_i - x_{BD}(u)) - F_a h_i]^2}{\frac{4}{3}EBy_{BD}^3(u)} \cdot \frac{dx_{BD}(u)}{du} du \tag{22}$$

$$U_s = \int_0^{\rho\cos\alpha} \frac{1.2{F_b}^2}{4GBy_{AB}(u)} \cdot \frac{dx_{AB}(u)}{du} du + \int_{\rho\cos\alpha}^{u(\theta-\gamma)} \frac{1.2{F_b}^2}{4GBy_{BD}(u)} \cdot \frac{dx_{BD}(u)}{du} du \tag{23}$$

$$U_a = \int_0^{\rho\cos\alpha} \frac{{F_a}^2}{4EBy_{AB}(u)} \cdot \frac{dx_{AB}(u)}{du} du + \int_{\rho\cos\alpha}^{u(\theta-\gamma)} \frac{{F_a}^2}{4EBy_{BD}(u)} \cdot \frac{dx_{BD}(u)}{du} du \tag{24}$$

where

$$u(\theta - \gamma) = (\theta - \gamma) r \sin^2\alpha + (\rho\cos^2\alpha + h\sin\alpha)\cos\alpha \tag{25}$$

$$\alpha_i = \arccos\frac{r_b}{r_i} \tag{26}$$

$$d_i = r_i\cos\gamma - r_f\cos\theta \tag{27}$$

$$\gamma = \frac{\pi}{Z} \cdot \frac{\pi + 4e * \tan\alpha}{2\pi} + inv\alpha - inv\alpha_i \tag{28}$$

$$h_i = r_i\sin\gamma \tag{29}$$

$$\beta = \alpha_i - \gamma \tag{30}$$

Therefore, the mesh stiffness can be expressed as a function of r_i, which denotes the distance from gear center to a contact point on tooth flank profile. In order to facilitate the observation for TVMS, the stiffness can also be represented as a function of ϕ, the rotation angular displacement of the driving gear, by using the following equation.

$$\phi = \frac{\sqrt{r_i^2 - r_b^2} - \sqrt{r_C^2 - r_b^2}}{p_b} \cdot \frac{360}{Z} \tag{31}$$

where p_b denotes the pinion base pitch, r_i means the distance between the contact point and the pinion center. ϕ can be calculated when the meshing engagement of the tooth starts.

3.4 Hertzian stiffness

According to the research by Yang and Sun [28], the Hertzian contact stiffness of a pair of meshing teeth, k_h, is virtually constant along the whole action line independent of both the interpenetration depth and the contact position. k_h can be expressed as

$$k_h = \frac{\pi b}{2}\left(\frac{1 - {v_1}^2}{E_1} + \frac{1 - {v_2}^2}{E_2}\right)^{-1}. \tag{32}$$

where b is the tooth width; E_1, E_2 and v_1, v_2 denote elastic moduli and Poisson's ratios of the pinion and wheel, respectively.

3.5 Stiffness considering fillet-foundation deflection

In addition to deformation of gear tooth, fillet-foundation deflection, δ_f, also affects the gear mesh stiffness. The derived analytical formula for δ_f was proposed by Sainsot and Velex [20] on the basis of the theory of Muskhelishvili [29].

$$\delta_f = \frac{F}{k_f} = \frac{F\cos^2\beta}{Eb}\{L^*(\frac{u_f}{S_f})^2 + M^*(\frac{u_f}{S_f}) + P^*(1 + Q^*\tan^2\beta)\} \tag{33}$$

where k_f is the corresponding fillet-foundation deflection stiffness, b is the tooth width, β is the load angle. Parameters u_f and S_f are defined in Figure 6. The coefficients L^*, M^*, P^* and Q^* can be computed according to the following polynomial functions [20],

$$X^*(h_f, \theta_f) = \frac{A_i}{\theta_f^2} + B_i h_f^2 + \frac{C_i h_f}{\theta_f} + \frac{D_i}{\theta_f} + E_i h_f + F_i \tag{34}$$

X^* indicates the coefficients L^*, M^*, P^* and Q^*; r_f, r_{int} and θ_f are given in Figure 6; $h_f = r_f / r_{\text{int}}$; the values of A_i, B_i, C_i, D_i, E_i and F_i are listed in Table 1.

3.6 Overall mesh stiffness

Contact ratio of spur gears is generally between 1 and 2, but for high contact ratio gear pairs it may be between 2 and 3. Thus, the number of tooth pair in contact varies between 1 and 2 or 2 and 3 alternatively during meshing. For a single tooth pair in contact, the total mesh stiffness can be

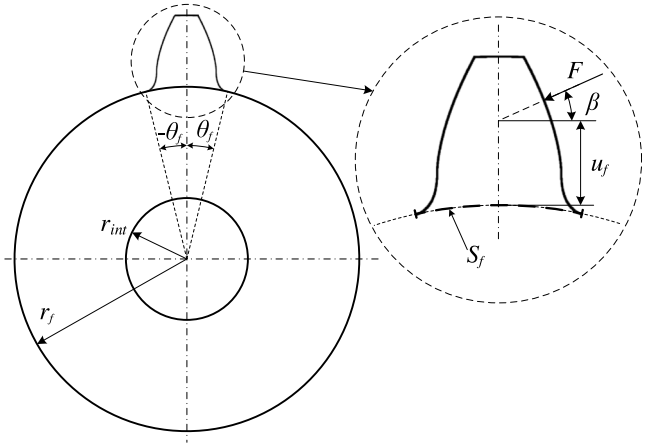

Fig. 6. Geometrical parameters of gear body and tooth for the fillet-foundation deflection [13].

obtained by

$$k_t = \frac{1}{\frac{1}{k_{b1}} + \frac{1}{k_{s1}} + \frac{1}{k_{a1}} + \frac{1}{k_{f1}} + \frac{1}{k_{b2}} + \frac{1}{k_{s2}} + \frac{1}{k_{a2}} + \frac{1}{k_{f2}} + \frac{1}{k_h}} \quad (35)$$

where subscripts 1, 2 indicate the pinion and wheel, respectively. When there are double or triple tooth pairs in contact instantaneously, the overall effective mesh stiffness is the sum of all the meshing pairs' stiffnesses and can be calculated as

$$k_t = \sum_{i=1}^{n} k_{t,i} = \sum_{i=1}^{n} \frac{1}{\frac{1}{k_{b1,i}} + \frac{1}{k_{s1,i}} + \frac{1}{k_{a1,i}} + \frac{1}{k_{f1,i}} + \frac{1}{k_{b2,i}} + \frac{1}{k_{s2,i}} + \frac{1}{k_{a2,i}} + \frac{1}{k_{f2,i}} + \frac{1}{k_{h,i}}} \quad (36)$$

where n denotes the number of meshing tooth pairs, and $i=1$, $i=2$ and $i=3$ represent the first, the second and the third meshing tooth pair, respectively.

4 Discussion

4.1 Finite element modeling

In many earlier literatures [3,7,13], in order to simplify the calculation of tooth deflection, only one pair of teeth was considered. The same simplification which is widely accepted in existing work is still introduced in the present study. 3D models are employed to model spur gear pairs using finite element software ABAQUS. The 3D models are meshed with 10-node modified quadratic tetrahedron elements. Coupling constraint is added between centerline and hub of the pinion. Displacement type boundary condition is set for pinion centerline with only one degree of freedom (DOF) parallel to the action line. Therefore, the pinion hub only has the same translational DOF. A linear distributed load, F, is introduced by its two projections on the **i** axis and **j** axis and it is applied to the pinion axis. It simulates the meshing force and is parallel with the action line. All nodes of the wheel hub are restrained with no freedom. A general contact interaction is created between the two meshing teeth. A complete finite element model of a meshing tooth pair is shown in Figure 7. The element number of the model is 211386. After computation, the pinion center displacements δ_i and δ_j along the **i** axis and **j** axis, respectively, are obtained. The deflection of the meshing tooth pair along the action line is given by

$$\delta = \delta_i \cos\alpha + \delta_j \sin\alpha \quad (37)$$

The stiffness of a single meshing tooth pair is then computed as

$$k = F/\delta \quad (38)$$

The major parameters of a single-stage spur gear system introduced in this model are listed in Table 2. The diameters of inner bore of pinion and wheel are 20 mm and 30 mm, respectively. The listed pinion and wheel belong to R-B tooth and B-R tooth, respectively. In this way, the following study can investigate the influence of both R-B and B-R teeth on mesh stiffness determination.

Figure 8 shows the evolution of the single tooth pair mesh stiffness, k_t, computed by the proposed analytical and finite element models. The tool tip fillet radius ρ in Figure 8 is 0.38 m. The position where the tooth pair starts to engage is set as the initial position of the pinion. A good agreement between the results yielded by the FEM and the proposed model is obtained. The maximum difference between the mesh stiffnesses obtained by the two methods is 5.72%. Therefore, the effectiveness of the proposed analytical model for determining the mesh stiffness with considering root fillet area is verified.

4.2 Influence of actual root fillet area on gear mesh stiffness

The evolutions of single tooth pair mesh stiffness and TVMS yielded by models considering tooth root fillet area in different ways are compared, as illustrated in Figure 9a and b, respectively. Three models are involved. The first one is the simplified model with setting the studied gear tooth starting from the base circle [18]. This model ignored the gear tooth part between the root and base circles of an R-B tooth. Instead, for a B-R tooth, a tooth part of involute curve extension between the two circles is added. For the case in Table 2, the simplification on the tooth pair results in average increments of single tooth pair stiffness and TVMS about 14.5% and 14.1%, respectively, compared with those of the proposed model. This is because the simplification enhances the rigidity of the pinion tooth significantly, meanwhile, it brings a relatively small reduction of the rigidity of the wheel tooth. The second model [12] made some improvements on the first one with the introduction of simplified root fillets exhibited as straight line for R-B tooth and involute for B-R tooth. However, this model underestimated the stiffness for both the R-B and B-R teeth (decrease about 39% for both the

Table 1. Coefficients of the polynomial in Eq. (34).

	A_i	B_i	C_i	D_i	E_i	F_i
$L^*(h_f,\theta_f)$	-5.574×10^{-5}	-1.9986×10^{-3}	-2.3015×10^{-4}	4.7702×10^{-3}	0.0271	6.8045
$M^*(h_f,\theta_f)$	60.111×10^{-5}	28.100×10^{-3}	-83.431×10^{-4}	-9.9256×10^{-3}	0.1624	0.9086
$P^*(h_f,\theta_f)$	-50.952×10^{-5}	185.50×10^{-3}	0.0538×10^{-4}	53.300×10^{-3}	0.2895	0.9236
$Q^*(h_f,\theta_f)$	-6.2042×10^{-5}	9.0889×10^{-3}	-4.0964×10^{-4}	7.8297×10^{-3}	−0.1472	0.6904

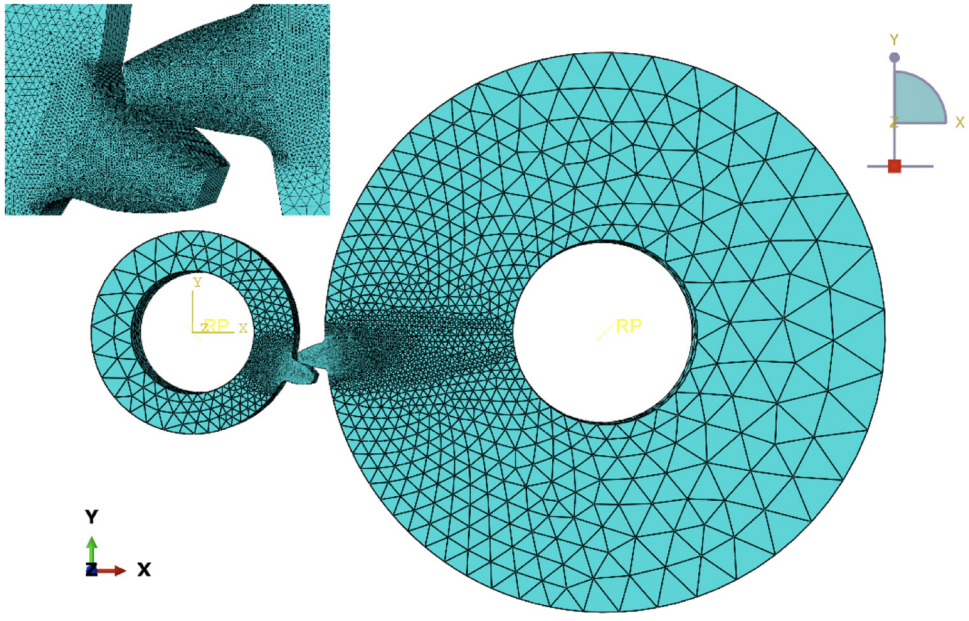

Fig. 7. Finite element model of a meshing tooth pair.

Table 2. Parameters of the gears.

	Pinion	Wheel
Teeth number	$Z_1=19$	$Z_2=48$
Module (mm)	$m=4$	$m=4$
Face width (mm)	$b=16$	$b=16$
Pressure angle (°)	$\alpha=20$	$\alpha=20$
Addendum coefficient	$h_a{}^*=1$	$h_a{}^*=1$
Tip clearance coefficient	$c^*=0.25$	$c^*=0.25$
Addendum modification coefficient	$e_1{}^*=0$, 0.1, 0.3, 0.5	$e_2{}^*=0$, −0.1, −0.3, −0.5
Tool tip radius coefficient	$\rho_1{}^*=0.38$	$\rho_2{}^*=0.38$
Modulus of elasticity (GPa)	$E_1=206.8$	$E_2=206.8$
Poisson's ratio	$v_1=0.3$	$v_2=0.3$

The asterisk represents the ratio of the parameter to modulue.

computed single tooth pair stiffness and TVMS). The deviations of the results obtained by the simplified methods comparing with those of the proposed analytical model demonstrate that it is of significant importance to consider gear tooth profile with actual root fillet area.

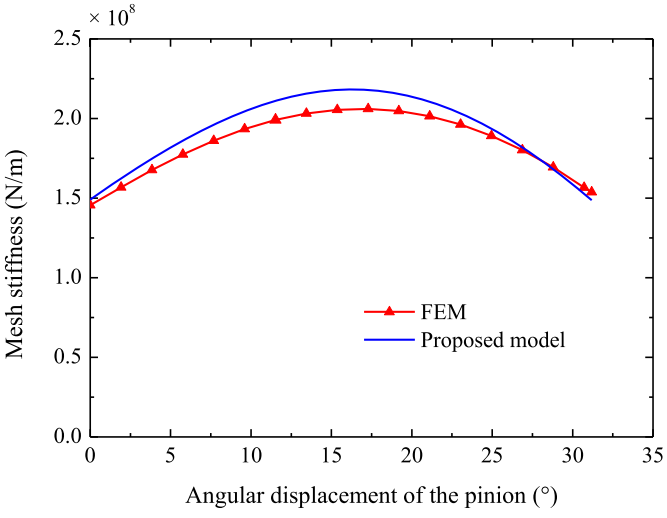

Fig. 8. Comparison between single tooth pair mesh stiffness evolutions yielded by the FEM and the proposed analytical model.

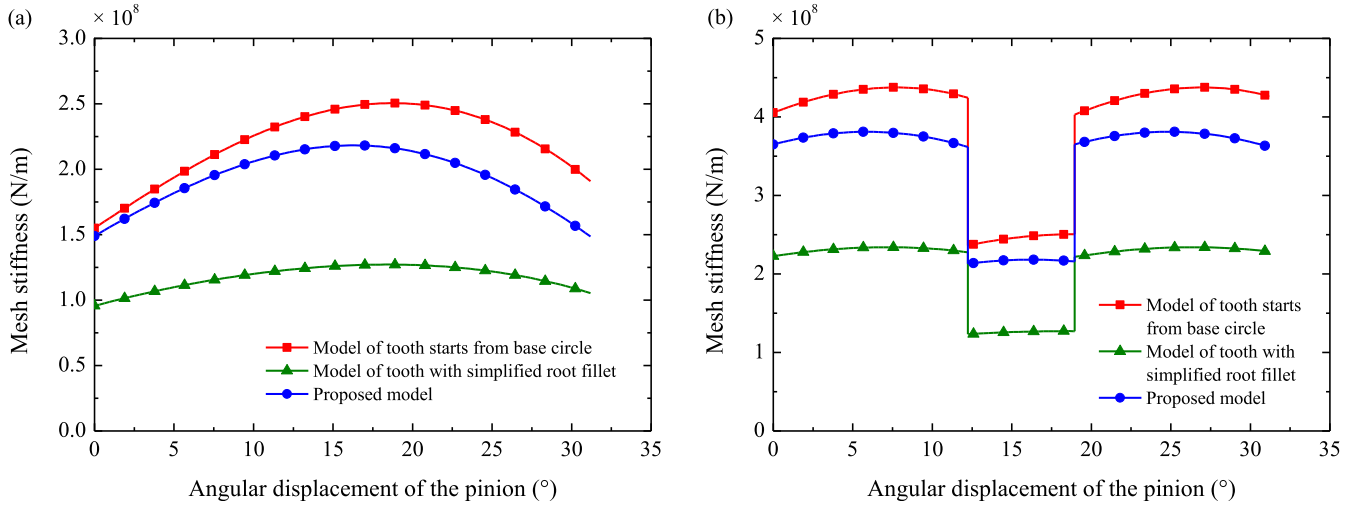

Fig. 9. Evolutions of gear mesh stiffness yielded by different models: (a) single tooth pair stiffness, (b) TVMS.

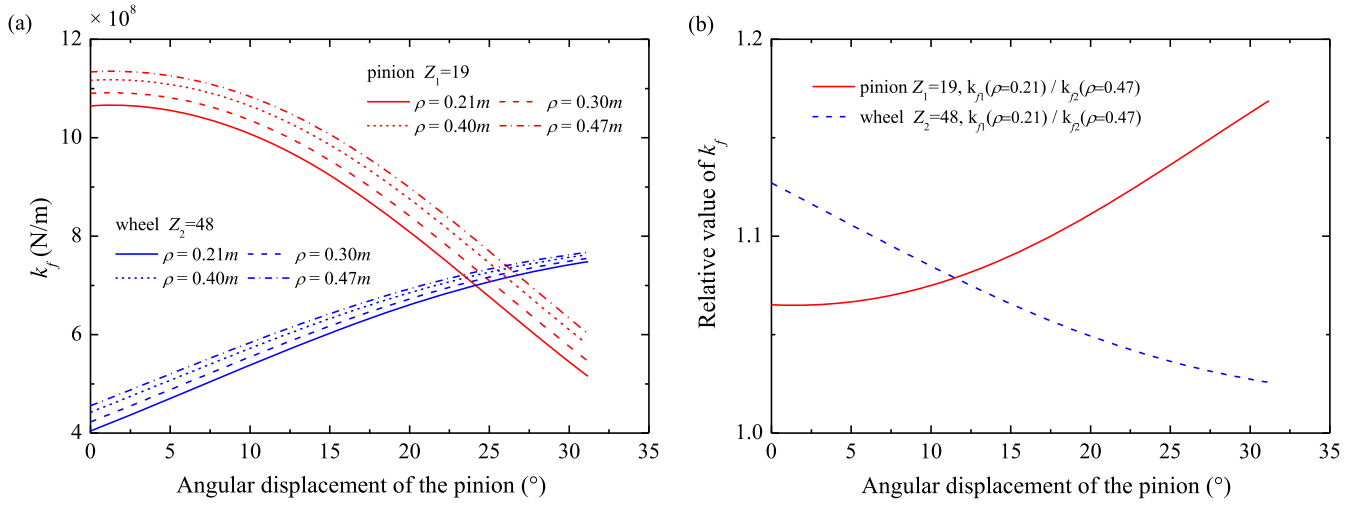

Fig. 10. Evolutions of (a) k_f, (b) relative value of k_f.

4.3 Influence of tool tip fillet radius on gear mesh stiffness

Tool tip fillet radius ρ, determining the value of S_f and θ_f in Figure 6, is an important factor for tooth fillet-foundation deflection stiffness k_f. According to constraint conditions defined in Section 2.1, $\rho = 0.21$–$0.47\,m$ and is applicable for the pinion–wheel set in Table 2. Figures 10a shows the evolutions of k_f of gears machined by tools with various tip fillet radius, while Figure 10b shows the evolutions of relative value of k_f that denotes the ratio of k_{f1} ($\rho = 0.47m$) to k_{f2} ($\rho = 0.21m$). The value of k_f declines with the decrease of tool tip fillet radius for both the pinion and wheel. The reduction of k_f for pinion is between 6.5% and 16.9%, while for wheel it is 2.6–12.7%. The influence of ρ on the pinion is more pronounced than on the wheel. The nearer the mesh point is to the tooth top, the greater k_f decreases. For a high contact ratio (HCR) gear pair of which $h_a{}^* = 1.33$ and $Z_1 = Z_2 = 48$, the feasible interval of ρ is $[0, 0.3]$. The corresponding evolutions are shown in Figure 11a and b. In addition to the aforesaid conclusions, we can observe that k_f of HCR gear pair is more susceptible to ρ.

The influence of tool tip fillet radius on the total mesh stiffness k_t of the machined gears (Table 2) is studied. The computational results are presented in Figure 12a and b. There is a reduction of stiffness when a gear pair machined by a tool with a relatively small tip fillet. Specifically, for single tooth pair mesh stiffness, the maximum and mean differences between gears cut by tools with $\rho = 0.21\,m$ and $0.45\,m$ are 5.94% and 5.21%, respectively. For the other stiffness, corresponding values are 5.36% and 5.18%, respectively. For the studied gear set, the analysis result suggests that an increase in tool tip fillet radius will augment the stiffness of the gear pair.

The evolutions of k_t are further compared between a HCR gear pair ($h_a{}^* = 1.33$, $Z_1 = Z_2 = 48$ and $\varepsilon = 2.252$) and a low contact ratio (LCR) gear pair ($h_a{}^* = 1$, $Z_1 = Z_2 = 48$ and $\varepsilon = 1.748$). Figure 13a and b show the evolutions of

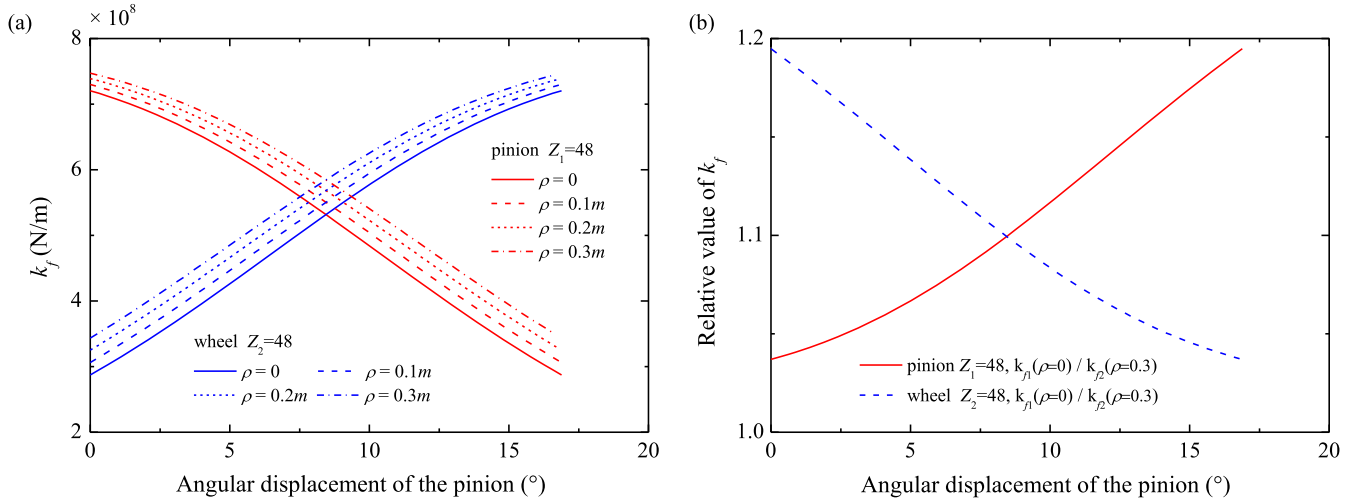

Fig. 11. Evolutions of (a) k_f and (b) relative value of k_f for a HCR gear pair.

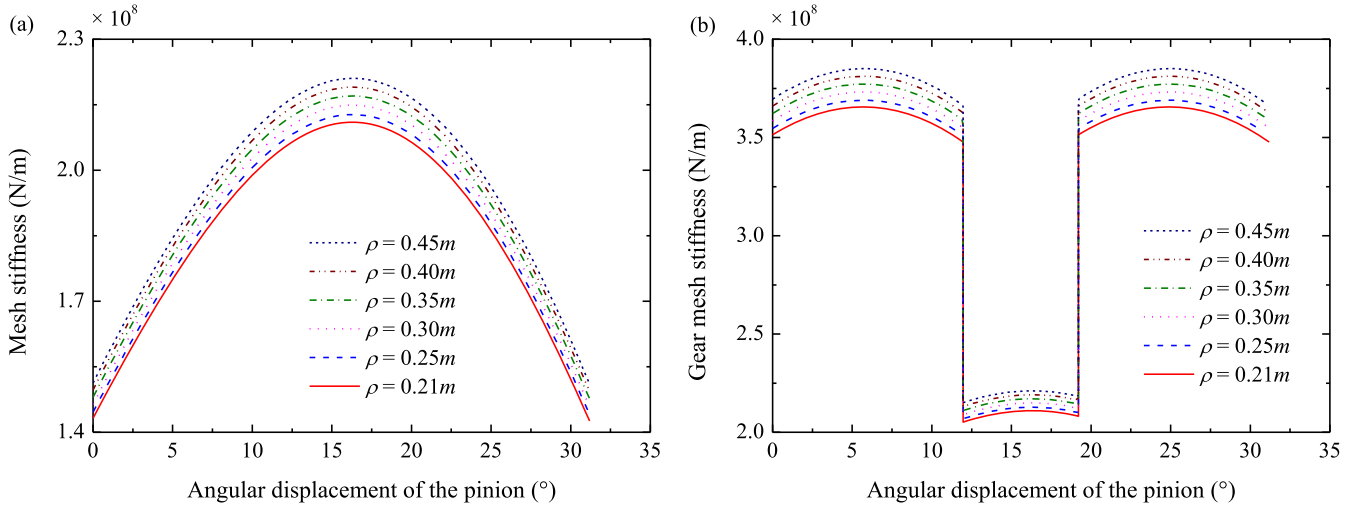

Fig. 12. Evolutions of gear mesh stiffness for different tool tip fillet radius: (a) single tooth pair stiffness, (b) TVMS.

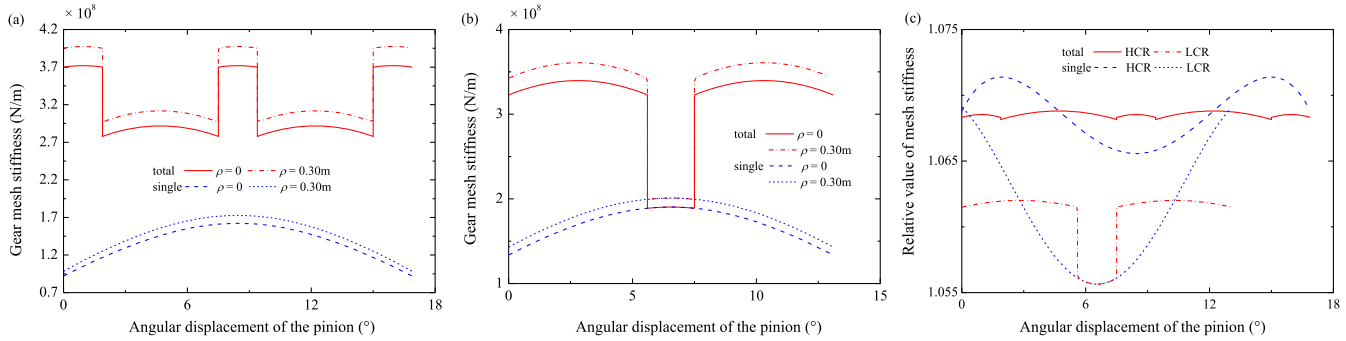

Fig. 13. Evolutions of gear mesh stiffness for different tool tip fillet radius: (a) HCR, (b) LCR, (c) relative value of mesh stiffness.

single tooth pair stiffness and overall stiffness for HCR and LCR gear pair, respectively. In Figure 13c, the relative values of k_t are shown. As the value of ρ increases from 0 to $0.3m$, the increment of overall mesh stiffness ranges from 6.8% to 6.9% and 5.6% to 6.2% for the HCR and LCR gear pair, respectively. We also find that k_t of a HCR gear pair is more susceptible to ρ than that of a LCR one.

4.4 Influence of addendum modification on mesh stiffness

Addendum modification, introduced by a rack-cutter with non-conventional settings, will change the gear tooth thickness and geometry of root fillet area. The variations of mesh stiffnesses with respect to different addendum

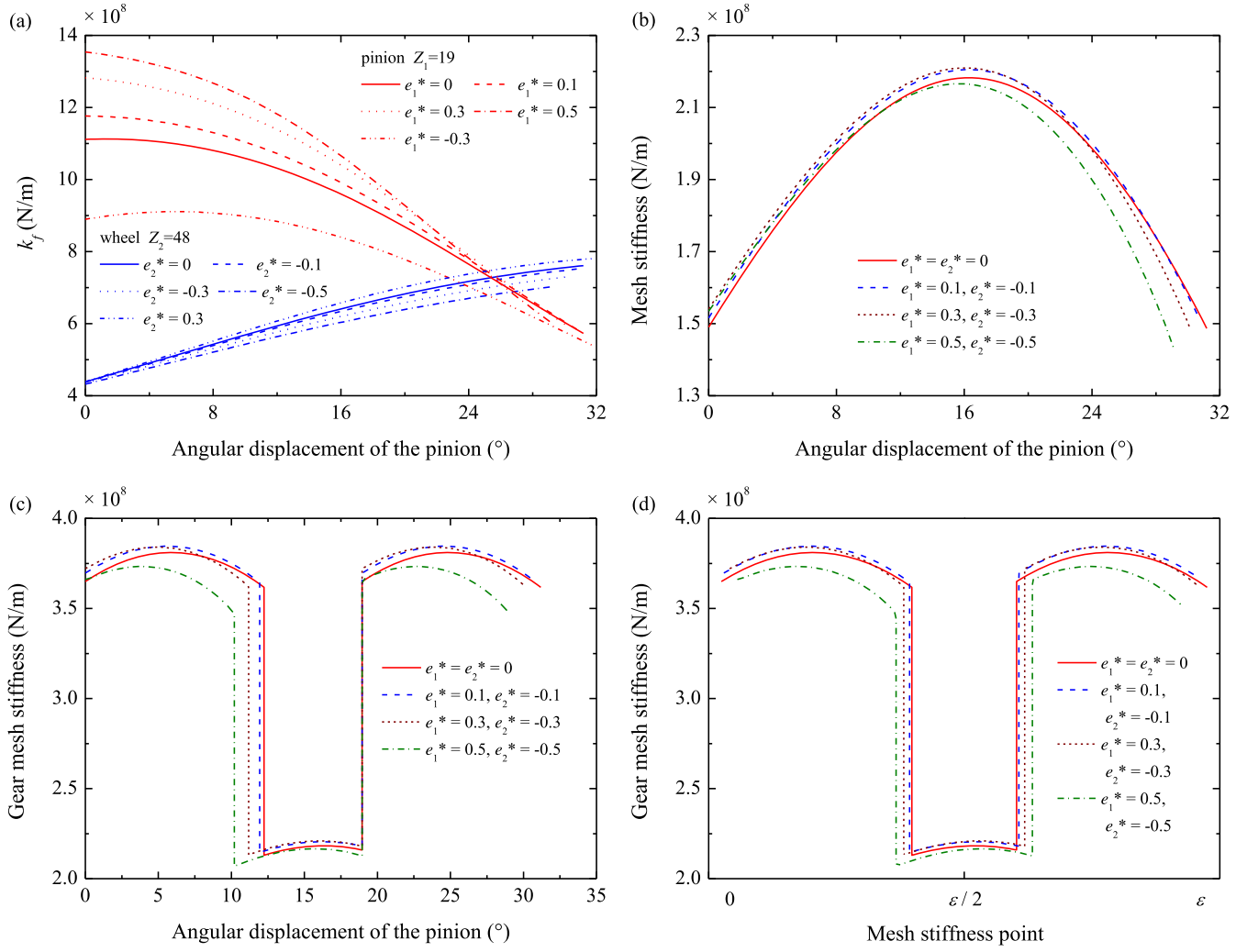

Fig. 14. Evolutions of gear mesh stiffness for different addendum modification coefficients: (a) k_f (b) single tooth pair stiffness (c) TVMS (d) TVMS.

modification coefficients, e_1* and e_2*, are illustrated in Figure 14a–d, respectively. The tool tip fillet radius coefficient $\rho = 0.38$ for all cases. Long-addendum brings an increment of k_f, while short-addendum results in a reduction of that. For the pinion, the rangeability of k_f resulted from the variation of addendum modification coefficient is greater than that of the wheel (Fig. 14a). The gear modification reduces contact ratio and changes the mesh stiffnesses (Fig. 14b). Modified gear pairs for both $e_1^* = 0.1$, $e_2^* = -0.1$ and $e_1^* = 0.3$, $e_2^* = -0.3$ have higher stiffnesses than a standard gear pair when they are at single-tooth-pair meshing stage (Figure 14c and d). However, greater modification coefficients, i.e., $e_1^* = 0.5$, $e_2^* = -0.5$, may also have an opposite influence on mesh stiffness when the gear pair varies from double-tooth-pair meshing stage to single-tooth-pair meshing stage.

4.5 Influence of tooth profile wear and modification on gear mesh stiffness

Early stage wear is inevitable for gear pairs. Although this kind of wear is always quite slight, it still leads to a decrease in gear mesh stiffness. Fortunately, wear cannot arise on root fillet area since contact does not take place in this region during meshing. Thus, the involute profile part BC (see Fig. 5) and the fillet of a wearing gear can still be obtained by using Eq. (13). For a pair of involute spur gears, the relative sliding velocity between the contact tooth flanks is proportional to the distance from contact point to pitch point. With the increase of sliding velocity, the tooth wear is likely to increase. Thus, the wear on tooth flank is usually nonuniform. Assuming that early wear along the tooth surface, shown in Figure 15a, is proportional to Δs. Set proportion coefficient as I_h. Then the contact zone (part CD) of involute profile should be acquired by following equations

$$\begin{cases} x'_{CD} = x_{CD} - \Delta h \sin \beta_u \\ y'_{CD} = y_{CD} - \Delta h \cos \beta_u \end{cases} \tag{39}$$

where $\Delta h = \Delta s I_h$, $\Delta s = |u - \rho \cos\alpha - h\tan\alpha| cot\alpha / \sin\alpha$, β_u means the angle between the normal direction of tooth flank and the axis y. $\sin\beta_u = \sin\alpha_i \cos\gamma - \cos\alpha_i \sin\gamma$, $\cos\beta_u = \cos\alpha_i \cos\gamma + \sin\alpha_i \sin\gamma$, $u \in [u_s, u_e]$.

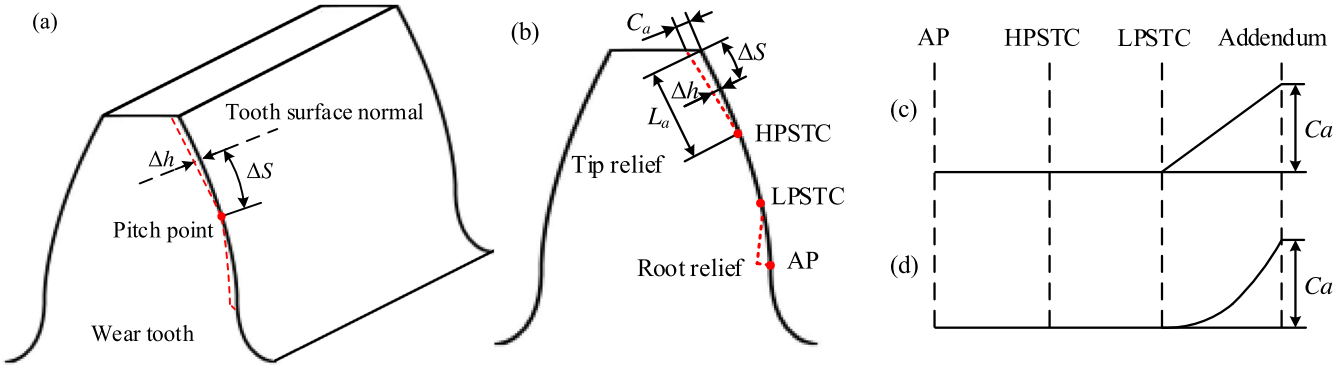

Fig. 15. Schematic diagram of a gear tooth with profile deviation: (a) wear, (b) tooth profile modification; K-chart: (c) linear modification, (d) parabolic modification.

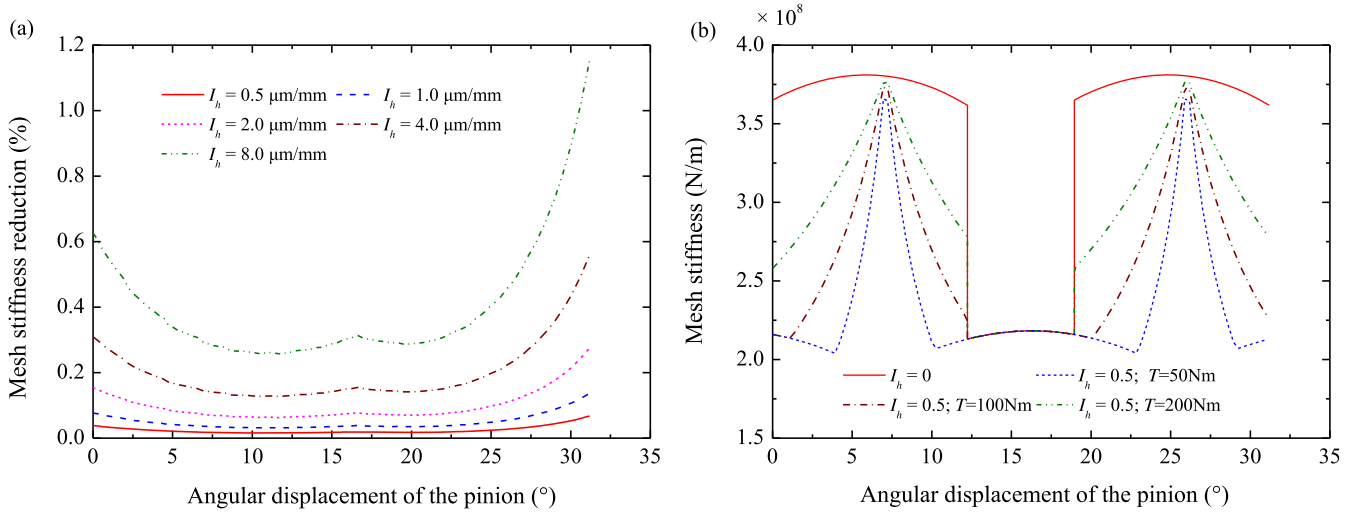

Fig. 16. Gear pair with different wear values: (a) single tooth pair stiffness reduction of nonuniform wear, (b) TVMS.

$$\sin\alpha_i = \frac{\sqrt{(x_{CD}+L)^2+y_{CD}{}^2-r_b{}^2}}{\sqrt{(x_{CD}+L)^2+y_{CD}{}^2}},\ \cos\alpha_i = \frac{r_b}{\sqrt{(x_{CD}+L)^2+y_{CD}{}^2}},$$

$$\sin\gamma = \frac{y_{CD}}{\sqrt{(x_{CD}+L)^2+y_{CD}{}^2}},\ \cos\gamma = \frac{x_{CD}+L}{\sqrt{(x_{CD}+L)^2+y_{CD}{}^2}}.$$

$$u_s = \rho\cos\alpha + h\tan\alpha - \frac{m}{2}\sin\ \alpha\ \tan\alpha$$

$$\left(\sqrt{Z_0^2\sin^2\alpha + 4Z_0h_a{}^* + 4h_a{}^{*2}} - Z_0\sin\alpha\right),\ u_e = (mh_a{}^* + h)$$

$\tan\alpha + \rho\cos\alpha$.

Tooth profile modification, shown in Figure 15b, is another important source producing profile deviation. Since root relief of one member has the same effect as tip relief of the mating member, tip reliefs on both the pinion and the wheel are adopted in this paper. All modifications start at the highest point of single tooth contact (HPSTC). The tip relief part of tooth profile can also be obtained by Eq. (40). Setting $\Delta h = C_a(\Delta s/L_a)^b$, where C_a and L_a are the amount and the length of profile modification, respectively, b = 1 for linear modification and b = 2 for parabolic modification.

For a gear pair with tooth deviations, such as profile nonuniform wear and modification, the overall mesh stiffness in double-tooth engagement can be obtained by the following formulas [25]

$$k_t = \frac{k_1+k_2}{1+k_2E_{12}/F_n}E_1 - E_2 = E_{12} < 0$$
$$k_t = \frac{k_1+k_2}{1-k_1E_{12}/F_n}E_1 - E_2 = E_{12} > 0 \quad (40)$$

where $E_1 = \Delta h_{p1} + \Delta h_{w1}$, $E_2 = \Delta h_{p2} + \Delta h_{w2}$. Subscripts 1 and 2 mean the first and the second tooth pair meshing at the same time, respectively.

The mesh stiffness influenced by nonuniform early stage wear of gear pairs can be obtained by using the developed method. It is assumed that the wear on both flanks of gear tooth is the same. For mating gear pairs made of the same material, the pinion usually gets worn more severely in that its tooth contact frequency is higher comparing with that of the mating gear. Therefore, I_h for the pinion should be larger than that for the wheel. In following cases, we apply I_h for the wheel and $I'_h = I_h z_2/z_1$ for the pinion. The reductions of single tooth pair mesh stiffness for gear pairs with nonuniform wears, in which I_h = 0.5–8 μm/mm, are shown in Figure 16a. The maximum wear appears on tooth tip of the

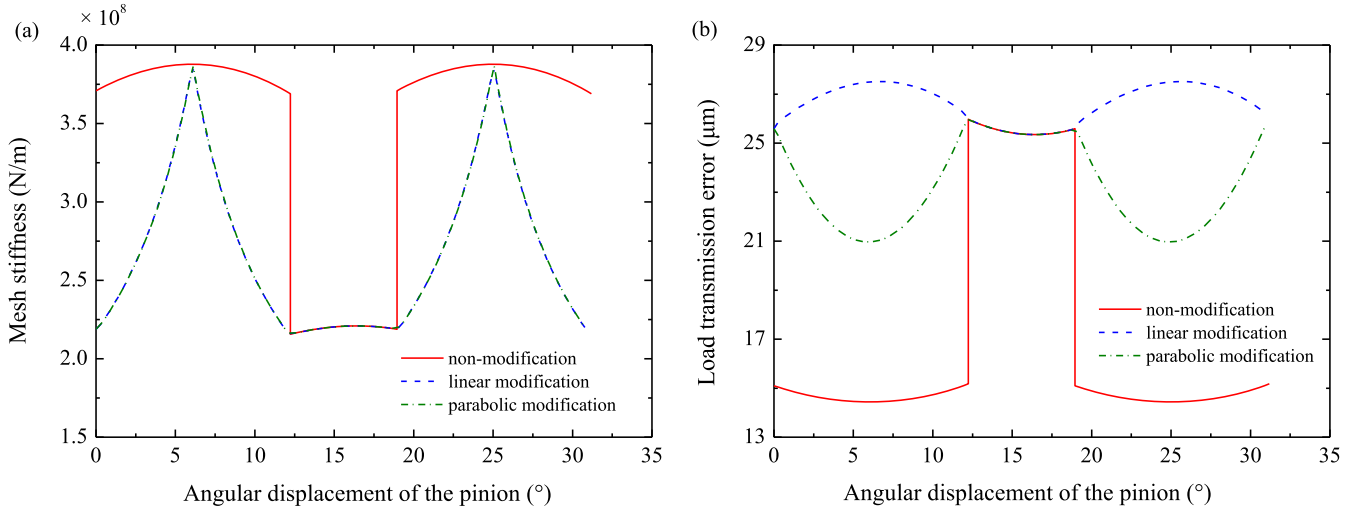

Fig. 17. Gear pair with different profile modifications: (a) TVMS, (b) load transmission error.

wheel and the approach point (AP) of the pinion tooth. When I_h ranges from 0.5 to 6 μm/mm, the maximum wear is 5.16–82.56 μm. The tool tip fillet radius coefficient is fixed at 0.38. An increase in wear value results in severer reductions of mesh stiffnesses. However, a nonuniform wear causes decreases of mesh stiffness in various degrees at different meshing points. The reduction is the largest while the pinion tooth is engaging out. Figure 16b shows the evolutions of the overall mesh stiffness of gear pairs. In spite of only a little change of the single tooth mesh stiffness, a significantly reduction of overall mesh stiffness in double-tooth engagement is generated form the profile deviations due to wear and it decreases with the applied load increasing.

For the cases simulated in this paper, the applied load $T = 200$ Nm, the amount of profile modification $C_a = 25.94$ μm, $C_a = 26.29$ μm for the pinion and the wheel, respectively. Evolutions of TVMS and load transmission errors of gear pairs with different profile modifications are shown in Figure 17a and b, respectively. Although the reductions of single tooth mesh stiffness due to tip relief are less than 0.1%, the total mesh stiffness in double tooth contact duration decrease obviously in Figure 17a. In this paper, evolutions of TVMS for both the linear and the parabolic modification tooth pair are almost equal to each other. However, the corresponding load transmission errors are quite different. The transmission error variations of modified gear pairs are obviously smaller than that of a non-modified gear pair, which helps to deduct vibration and noise.

5 Conclusion

In this article, an analytical model for evaluating mesh stiffness of gear pairs machined by a rack-type cutter considering actual tooth profile geometry was proposed. Related formulations are derived according to axial compressive, bending, shear, Hertzian contact and fillet-foundation deflection stiffnesses. A comparison between the stiffness results from the proposed model and FEM verified the effectiveness of the new model. The following conclusions are obtained:

- It is of significant importance to model the gear tooth starting from the dedendum circle with actual root fillet area for an accurate evaluation of gear mesh stiffness.
- The TVMS decreases with the increasing of tool tip fillet radius. TVMS of a HCR gear pair is more susceptible to tool tip fillet radius than that of a LCR one.
- Long-addendum brings an increment of k_f, while short-addendum results in a reduction of that. The addendum modification of gear pairs reduces contact ratio and changes gear mesh stiffness. Appropriately addendum modified gear pair may have higher mesh stiffnesses than a standard one.
- An increase in wear value leads to severer reduction of mesh stiffness. A nonuniform wear causes obviously decreases of mesh stiffness in double tooth contact duration.
- Tooth profile modifications decrease the gear mesh stiffness. Different forms of profile modification have the same influence on TVMS, but they will produce diverse load transmission errors.

Nomenclature

A_x	Area of the section where the distance to the gear root is d_i, mm^2
b	Width of the gear tooth, mm
d_i	Distance between the contact point and the tooth root, mm
E	Elastic modulus, GPa
e^*	Modification coefficient
F	Action load, N
G	Shear modulus, GPa
h	Distance between tool fillet and tool middle-line, mm
h_i	Distance between contact point and the tooth central line, mm

h_{a_*} Addendum, mm
h_a^* Addendum coefficient
h_f Dedendum, mm
h_f^* Dedendum coefficient
I_x Area moment of inertia of the section where the distance to the gear root is d_i, mm^4
k_a Radial compression stiffness, N/mm
k_b Bending stiffness, N/mm
k_f Stiffness considering fillet-foundation deflection, N/mm
k_h Hertzian contact stiffness, N/mm
k_s Shear stiffness, N/mm
k_t Overall mesh stiffness, N/mm
m Module, mm
p_b Base pitch of pinion
r Reference radius, mm
r_b Base radius, mm
r_B Distance between the gear center and the end point of root fillet curve, mm
r_f Root radius, mm
r_i Distance from gear center to contact point on tooth flank profile, mm
u Parameter of rack-cutter flank profile equations
v Poisson's ratio
Z Number of teeth
Z_0 Number of teeth on a mating gear of the gear being generated
α Profile angle of the rack cutter, rad
α_B Pressure angle at starting point of the contact zone (point B), rad
α_i Pressure angle at contact point, rad
β Load angle (angle of the force component F_b and the force F), rad
β_u Angle between the normal of tooth flank and the axis y, rad
γ Angle between tooth symmetrical line and the connection between gear center and contact point, rad
δ Deformation of the contact teeth due to the force F, mm
Δ Distance between tool tip fillet arc center and tool symmetric line, mm
Δh Uniform wear along the tooth surface, mm
Δs Distance between contact point and reference point, mm
θ Half tooth angle on the root circle, rad
ρ Tool tip radius, mm
ρ^* Tool tip radius coefficient
φ Angle of coordinate system S_2 rotation, rad
ϕ Rotation angular displacement of the driving gear, degree

Acknowledgment. The authors would like to acknowledge the support from National Natural Science Foundation of China (Grant Nos. 51405316, 51435001). Q.Z. and Y.H. would like to acknowledge the supports from the Starting Foundation of Sichuan University (No. 2017SCU12021) and the Aeronautical Science Foundation of China (No. 20160219001).

References

[1] T. Nishino, Integrated excitation models of the helical gear system, ASME Design Engineering Technical Conferences, No. DETC2007-34134, Las Vegas, NV, 2007
[2] J.T. Alves, J. Wang, M. Guingand, J.P. Vaujany, P. Velex, Static and dynamic models for spiral bevel gears, Mech. Ind. 13 (2012) 325–335
[3] F. Chaari, W. Baccar, M.S. Abbes, M. Haddar, Effect of spalling or tooth breakage on gearmesh stiffness and dynamic response of a one-stage spur gear transmission, Eur. J. Mech. A Solid 27 (2008) 691–705
[4] X. Zhou, Y. Shao, Y. Lei, M.J. Zuo, Time-varying meshing stiffness calculation and vibration analysis for a 16DOF dynamic model with linear crack growth in a pinion, J. Vib. Acoust. 134 (2012) 1–11
[5] ISO Standard 6336-2: 1996, Calculation of Load Capacity of Spur and Helical Gears-Part 2: Calculation of Surface Durability (Pitting), International Organization for Standardization, Geneva, Switzerland, 1996
[6] AGMA Standard 2001-D04, Fundamental rating factors and calculation methods for involute spur and helical gear teeth, American gear manufacturers association, Alexandria, VA, 2004
[7] M. Pimsarn, K. Kazerounian, Efficient evaluation of spur gear tooth mesh load using pseudo-interference stiffness estimation method, Mech. Mach. Theory, 37 (2002) 769–786
[8] Y. Pandya, A. Parey, Failure path based modified gear mesh stiffness for spur gear pair with tooth root crack, Eng. Fail. Anal. 27 (2013) 286–296
[9] O.D. Mohammed, M. Rantatalo, J. Aidanpaa, Improving mesh stiffness calculation of cracked gears for the purpose of vibration-based fault analysis. Eng. Fail. Anal. 34 (2013) 235–251
[10] T. Lin, H. Ou, R. Li, A finite element method for 3D static and dynamic contact/impact analysis of gear drives, Comput. Methods Appl. Mech. Eng. 196 (2007) 1716–1728
[11] H. Ma, X. Pang, R. Feng, R. Song, B. Wen, Fault features analysis of cracked gear considering the effects of the extended tooth contact. Eng. Fail. Anal. 48 (2015) 105–120
[12] X. Liang, M. Zuo, M. Pandey, Analytically evaluating the influence of crack on the mesh stiffness of a planetary gear set, Mech. Mach. Theory 76 (2014) 20–38
[13] F. Chaari, T. Fakhfakh, M. Haddar, Analytical modelling of spur gear tooth crack and influence on gearmesh stiffness, Eur. J. Mech. A Solid 28 (2009) 461–468
[14] J.I. Pedrero, M. Pleguezuelos, M. Artés, J.A. Antona, Load distribution model along the line of contact for involute external gears, Mech. Mach. Theory, 45 (2010) 780–794.
[15] A. Fernandez del Rincon, F. Viadero, M. Iglesias, P. García, A. de-Juan, R. Sancibrian, A model for the study of meshing stiffness in spur gear transmissions, Mech. Mach. Theory 61 (2013) 30–58
[16] H. Ma, X. Pang, R. Feng, J. Zeng, B. Wen, Improved time-varying mesh stiffness model of cracked spur gears, Eng. Fail. Anal. 55 (2015) 271–287
[17] D.C.H. Yang, J.Y. Lin, Hertzian damping, tooth friction and bending elasticity in gear impact dynamics, J. Mech. Transm-T. ASME 109 (1987) 189–196

[18] X. Tian, M.J. Zuo, K. Fyfe, Analysis of the vibration response of a gearbox with gear tooth faults, ASME international mechanical engineering congress and exposition, Anaheim, California, USA, 2004
[19] A. Saxena, A. Parey, M. Chouksey, Time varying mesh stiffness calculation of spur gear pair considering sliding friction and spalling defects, Eng. Fail. Anal. 70 (2016) 200–211
[20] P. Sainsot, P. Velex, Contribution of gear body to tooth deflections – a new bidimensional analytical formula, J. Mech. Des. 126 (2004) 748–752
[21] X. Liang, H. Zhang, L. Liu, M. Zuo, The influence of tooth pitting on the mesh stiffness of a pair of external spur gears, Mech. Mach. Theory 106 (2016) 1–15
[22] F.L. Litvin, A. Fuentes, Gear geometry and applied theory, 2nd ed. Cambridge University Press, Cambridge, 2004.
[23] W. Yu, Y. Shao, C.K. Mechefske, The effects of spur gear tooth spatial crack propagation on gear mesh stiffness, Eng. Fail. Anal. 54 (2015) 103–119
[24] S. Feng, J. Mao, Y. Xie, Analysis and calculation of gear mesh stiffness with tooth wear, J. Mech. Eng. 51 (2015) 27–32
[25] Z. Chen, Y. Shao, Mesh stiffness calculation of a spur gear pair with tooth profile modification and tooth root crack, Mech. Mach. Theory, 62 (2013) 63–74
[26] X. Wu, Gear meshing principle, Xi'an Jiao Tong University press, Xi'an, 1982
[27] Z. Xu, Elasticity, 4th ed. Higher Education Press, Beijing, 2006
[28] D.C.H. Yang, Z.S. Sun, A rotary model for spur gear dynamics, J. Mech. Transm-T ASME 107 (1985) 529–535
[29] N.I. Muskhelishvili, Some basic problems of the mathematical theory of elasticity, Springer Science & Business Media, 1977

Cite this article as: Y. Yang, J. Wang, Q. Zhou, Y. Huang, J. Zhu, W. Yang, Mesh stiffness modeling considering actual tooth profile geometry for a spur gear pair, Mechanics & Industry **19**, 306 (2018)